

# Design of a Diaphragm Pump under Uncertainties using the Continuous Adjoint to the Cut-Cell Method

Konstantinos D. Samouchos <sup>1</sup>, Dimitrios H. Kapsoulis <sup>1</sup>,  
Xenofon S. Trompoukis <sup>1</sup>, and Kyriakos C. Giannakoglou <sup>1</sup>

<sup>1</sup> *National Technical University of Athens (NTUA), School of Mechanical Engineering,  
Parallel CFD & Optimization Unit, Athens, Greece,  
ksamouchos@yahoo.com, jim.kapsoulis@gmail.com, vaggelisp@gmail.com,  
kgianna@central.ntua.gr*

---

## Abstract

This paper is on the development of the unsteady continuous adjoint method associated with a flow solver based on the cut-cell method to be used for the optimization of a diaphragm pump. A key feature of this pump is the oscillating diaphragm which can properly be handled by the cut-cell method on a stationary Cartesian grid, dynamically adapted to the moving diaphragm. In both the flow and adjoint solvers, emphasis is laid on the proper treatment of cells that appear in or disappear from the fluid domain, due to the motion of the diaphragm. The continuous adjoint method is implemented to compute the derivatives of an integral measuring the backflow along the outlet with respect to parameters controlling the shape of the stationary part of the pump.

In the second part of this paper, the developed adjoint method is used for the shape optimization of the same pump under uncertainties. For the quantification of uncertainties, the non-intrusive Polynomial Chaos Expansion (PCE) method is used. The new objective function includes the mean value and the standard deviation of the quantity of interest used as objective function in the previous optimization without uncertainties. The adjoint solver for the case without uncertainties is also used for the gradient computation at the Gauss quadrature nodes, in the presence of uncertainties.

*Keywords:* Diaphragm pumps, Uncertainty Quantification, Polynomial Chaos Expansion, Cut-Cell Method, Continuous Adjoint Method

---

## 1. Introduction

This paper presents the shape optimization without and with uncertainties of a diaphragm pump [1], the main characteristic of which is the lack of rotating parts. Instead, its operation is based on the periodic motion of a diaphragm which is the driving force of the passing flow. Depending on the geometry and the diaphragm motion characteristics, these pumps often suffer from undesirable backflow at the exit, during a percentage of their period; the purpose of this

paper is to minimize and, hopefully, reduce backflow by redesigning the ducts of such a pump.

10 A prerequisite for the optimization process is the numerical simulation of the flow. Several methods to cope with the numerical simulation of time-dependent flows involving moving boundaries, such as deforming grids [2], overset grids [3], and immersed boundary methods (IBM) [4] can be found in the literature. The first method makes use of body-fitted grids and, thus, needs costly grid  
15 deformation processes to follow the boundary motion. On the other hand, with overset methods, the accurate application of the conservation laws calls for complex interpolations of the flow quantities. The IBM, introduced by Peskin [5], enjoy the advantages of Cartesian grids, i.e. simplicity in grid generation and deformation. The cut-cell method [6, 7, 8] is one of the most popular  
20 IBM methods which guarantees the satisfaction of the conservation laws. This is achieved by reshaping cells intersected by the solid boundary (cut-cells) by discarding their part belonging to the solid body. In this paper, the cut-cell method is developed and used for unsteady 2D laminar flows of incompressible fluids such as those occurring in diaphragm pumps, allowing grid refinement  
25 and dynamic adaptation.

Uncertainties related to the operating conditions of the pump are also taken into account. Uncertain variables are related to the inlet total pressure and the outlet static pressure. The scope is to design a shape which performs efficiently even with varying flow conditions. To this end, the objective function  
30 is expressed as a linear combination of the mean value  $\mu_F$  and the standard deviation  $\sigma_F$  of the quantity of interest (QoI). To compute these statistical moments, stochastic methods, such as Monte-Carlo (MC) [9], can be used at high computational cost though. Much cheaper is the Method of Moments which uses the adjoint method to compute the first- and second-order derivatives of  
35 the QoI with respect to (w.r.t.) the uncertain variables, in terms of which the statistical moments are expressed [10].

Herein, the PCE technique [11, 12] is used for the same computation. The method can be implemented intrusively (by deriving and solving new partial differential equations) or non-intrusively. In the latter, which is used in this  
40 paper, the Gauss integration rules determine a set of Gaussian nodes to be evaluated on the CFD solver. Then, the statistical moments are computed as the weighted sum of the computed QoI values at these nodes.

To perform the optimization, the continuous adjoint method [13] computes the derivatives of the QoI which is an outlet backflow metric w.r.t. the design  
45 variables controlling the pump shape. The derivation of the adjoint problem is presented in detail. Similarly to the flow equations, the cut-cell method is used to solve the adjoint equations. A combination of the adjoint method and the non-intrusive PCE technique is used to compute the derivatives of the objective function under uncertainties (being equal to the weighted sum of QoI at selected  
50 operating points) w.r.t. the design variables.

## 2. Grid Generation for the Cut-Cell Method

The generation of the computational grid for the cut-cell method [8] is based on the quad-tree data structure for minimum computational cost and memory usage [14]. For each cell, a unique pair of integers  $(i, j)$  is given, facilitating the computation of geometric quantities, such as cell volumes and barycentric coordinates. Starting from a single cell containing the whole domain, each cell cut by the geometry is subdivided into four quadrants, until some stopping criteria be met. During the grid generation process, the volume of all cells should be kept between user-defined upper and lower bounds. A key rule is that cell faces cannot have more than two neighbors. This rule prevents the formation of neighboring cells differing a lot in size, to avoid numerical instabilities. Two additional rules should be also satisfied: each edge can be intersected only once by the solid wall and cells are not allowed to have all of their edges intersected by the wall. By following these rules and after discarding the grid laying on the solid domain, cut-cells belonging to the fluid domain can be triangles, quadrilaterals or pentagons.

In order to increase the accuracy of the unsteady flow simulation around moving solid bodies, the grid must continuously be adapted close to the changing boundaries. Each time the boundary moves to its new position, cells close to the previous boundary position with area smaller than a threshold value are merged with their neighbors. Starting from the just coarsened grid, cells are re-subdivided in the vicinity of the displaced wall. Since different grids are used per time-step, the flow solution is transferred from the old to the new grid. During refinement, a 2D cell is decomposed into four smaller cells and each of them takes on the velocity values of its predecessor. During coarsening, four cells are merged to form a single new cell, the velocity values of which are equal to the average of the values of the four cells, weighted by their volumes. More details about grid generation and adaptation can be found in [8].

## 3. Flow Equations and Discretization

Using the pseudo-compressibility method [15, 16], the Navier-Stokes equations for unsteady ( $t$  is the real time) 2D laminar flows of incompressible fluids are written, using the Einstein notation, as

$$\Gamma_{ij}^{-1} \frac{\partial V_j}{\partial \tau} + \underbrace{\frac{\partial U_i}{\partial t} + \frac{\partial f_{ik}^{inv}}{\partial x_k} - \frac{\partial f_{ik}^{vis}}{\partial x_k}}_{R_i} = 0, \quad i = 1, 3 \quad (1)$$

where  $k = 1, 2$  refers to the Cartesian directions;  $(x_1, x_2)$  stand for  $(x, y)$  and  $(u_1, u_2)$  to the corresponding Cartesian velocity components.  $\vec{V} = [p \ u_1 \ u_2]^T$ ,  $\vec{U} = [0 \ u_1 \ u_2]^T$ ,  $\vec{f}_k^{inv} = [u_k \ u_1 u_k + p \delta_k^1 \ u_2 u_k + p \delta_k^2]^T$ ,  $\vec{f}_k^{vis} = [0 \ \tau_{1k} \ \tau_{2k}]^T$ , where  $\delta_i^j$  is the Kronecker symbol,  $p$  is the pressure divided by the density,  $\tau$  is

the pseudo-time,  $\tau_{ik} = \nu(\frac{\partial u_i}{\partial x_k} + \frac{\partial u_k}{\partial x_i})$ ,  $R_i$  is the non-preconditioned instantaneous residual of the equation and

$$\Gamma = \begin{bmatrix} \beta^2 & 0 & 0 \\ u_1 & 1 & 0 \\ u_2 & 0 & 1 \end{bmatrix}$$

80 is the preconditioning matrix, where  $\beta$  is the pseudo-compressibility coefficient. The discretization of eqs. (1) is based on the cell-centered finite volume scheme. For cells intersected by the geometry, the integration volume consists of the cell part which lies in the fluid domain.

The integration of eqs. 1 over a finite volume  $\Omega$ , at time-step  $k+1$ , yields

$$\int_{\Omega_{k+1}} \left( \Gamma_{ij}^{-1} \frac{\partial V_j}{\partial \tau} + \frac{\partial U_i}{\partial t} \right) d\Omega + \int_{S_{k+1}} (f_{ik}^{inv} - f_{ik}^{vis}) n_k dS = 0 \quad (2)$$

85 where  $S_{k+1}$  is the cell boundary and  $\vec{n}$  its normal unit vector. The discretization of eqs. 2 is based on the MUSCL supported by the Roe [17] scheme.

The discretization of the "physical" time derivative of eqs. 2, should take the solid wall motion into account, due to which cells change in shape or occasionally migrate from the fluid to the solid domain and vice-versa. In all these cases, the following discretization, based on the Reynolds theorem,

$$\int_{\Omega_{k+1}} \frac{\partial U_i}{\partial t} d\Omega \simeq \frac{U_i^{k+1} - U_i^k}{\Delta t} \Omega_{k+1} \quad (3)$$

is applied, where  $u_{w,n}$  is the wall normal velocity, computed in a way ensuring the satisfaction of the geometric conservation law. It is reminded that, for each cell, only one face is allowed to move. For cells belonging to the solid domain at  $t_k$  and the fluid domain at  $t_{k+1}$ ,  $\Omega_k = 0$  in eq. 3. Fluid cells at 90  $t_k$  becoming entirely solid at  $t_{k+1}$  should merge their conservative values with those of neighboring cells, which remain fluid. An extra term ( $\sum_{solid} U_i^k \Omega_k$ ), with summation over all solidified cells embodied in them, is added to eq. 3.

#### 4. Adjoint Equations and Discretization

The purpose of the optimization of the diaphragm pump without uncertainties is to minimize, or even suppress, backflow occurring instantaneously in the exit duct. Subsequently, the space-time integral of the sign of the normal to the outlet velocity should be maximized, in the sense that the entire exit should have the same (outgoing) velocity sign. Assuming that the normal to the pump outlet ( $S_O$ ) is  $\vec{n} = (1, 0)$ , the objective function  $F$  (which becomes the QoI in the presence of uncertainties) is defined by the differentiable integral

$$F = \int_0^T \int_{S_O} \frac{u_1}{\sqrt{u_1^2 + \alpha}} dS dt \quad (4)$$

where  $T$  is the period of the diaphragm motion and  $\alpha$  is an infinitesimally small number. The coordinates of the polygon vertices creating the upstream and downstream ducts of the main body of the pump are the design variables ( $b_m$ ) of the optimization, fig. 1. The derivatives of  $F$  are computed by defining an

augmented objective function  $F_{aug} = F + \int_0^T \int_{\Omega} \Psi_i R_i(\vec{V}) d\Omega dt$ , where  $\Psi_i$ ,  $i=1, 3$

are the adjoint variable fields and  $\Omega$  the whole domain covered by the fluid. By differentiating  $F_{aug}$  w.r.t.  $b_m$  and setting the multipliers of  $\vec{V}$  variations in the space-time integrals equal to zero, the unsteady adjoint equations

$$\Gamma_{ji}^{-1} \frac{\partial \Psi_j}{\partial \tau} - \frac{\partial \bar{\Psi}_i}{\partial t} - A_{jik} \frac{\partial \Psi_j}{\partial x_k} - \frac{\partial}{\partial x_k} f_{ik}^{A,vis} = 0 \quad (5)$$

arise where  $\bar{\Psi} = [0 \ \Psi_2 \ \Psi_3]^T$ ,  $\bar{f}_k^{A,vis} = [0 \ \tau_{1k}^A \ \tau_{2k}^A]^T$ , and  $\tau_{ik}^A = \nu \left( \frac{\partial \Psi_{i+1}}{\partial x_k} + \frac{\partial \Psi_{k+1}}{\partial x_i} \right)$ .

95 The pseudo-time term is artificially added in eq. 5 for numerical stability reasons. By setting the adjoint velocity components ( $\Psi_2, \Psi_3$ ) over the wall surface equal to zero (adjoint wall boundary conditions), all the surface integrals along the solid wall containing variations of the flow variables w.r.t.  $b_m$  disappear and we get

$$\begin{aligned} \frac{\delta F}{\delta b_m} &= - \int_0^T \int_{S_w} (\Psi_1 n_i + f_{ik}^{A,vis} n_k) \frac{\partial u_i}{\partial x_l} \frac{\delta x_l}{\delta b_m} dS dt - \int_0^T \int_{S_{I,O}} \Psi_{i+1} \nu \frac{\delta}{\delta b_m} \left( \frac{\partial u_i}{\partial n} \right) dS dt \\ &- \int_0^T \int_{S_{I,O}} \Psi_{i+1} \nu \frac{\delta}{\delta b_m} \left[ \left( \frac{\partial u_k}{\partial n} n_i + \frac{\partial u_k}{\partial t} t_i \right) n_k \right] dS dt + \int_0^T \int_{S_{I,O}} \Psi_i \frac{\delta}{\delta b_m} (f_{ik}^{inv} n_k) dS dt \\ &+ \int_0^T \int_{S_{I,O}} f_{ik}^{A,vis} n_k \frac{\delta U_i}{\delta b_m} dS dt + \int_0^T \int_{S_O} \Phi \frac{\delta u_1}{\delta b_m} dS dt \end{aligned} \quad (6)$$

100 where  $\Phi = \frac{\partial F}{\partial u_1} = \frac{\alpha}{(u_1^2 + \alpha)^{3/2}}$ ,  $S_w$ ,  $S_I$ ,  $S_O$  stand for the wall, comprising moving and stationary walls where the no-penetration condition applies, inlet and outlet surfaces respectively and  $t_i$  are the components of the unit vector tangent to  $S_{I,O}$ . The first integral on the r.h.s. of eq. 6 does not contain derivatives in the flow quantities w.r.t.  $b_m$  and can easily be computed. All the other are

105 eliminated by imposing proper adjoint boundary conditions along  $S_I$  and  $S_O$ . The second and third integrals are eliminated by considering that  $\frac{\delta}{\delta b_m} \left( \frac{\partial u_i}{\partial n} \right) = 0$  and imposing  $\Psi_{i+1} t_i = 0$  along  $S_I$  and  $S_O$ . The last three integrals in eq. 6 are treated differently along the inlet and outlet and are written in the form

$$\int_0^T \int_{S_{I,O}} \Psi_i \frac{\partial (f_{ik}^{inv} n_k)}{\partial Q_j} \frac{\delta Q_j}{\delta b_m} dS dt + \int_0^T \int_{S_{I,O}} f_{ik}^{A,vis} n_k \frac{\partial U_i}{\partial Q_j} \frac{\delta Q_j}{\delta b_m} dS dt + \int_0^T \int_{S_O} \Phi \frac{\delta u_1}{\delta b_m} dS dt$$

where  $\vec{Q}$  is defined as  $\vec{Q} = [p_t \ a \ p]^T$  for the inlet and  $\vec{Q} = \vec{V}$  for the outlet. The total pressure ( $p_t$ ) and flow angle ( $a$ ) at the inlet and the static pressure at the outlet are the boundary conditions of the flow problem and are independent of the design variables  $b_m$ . Subsequently, these three integrals can be eliminated by setting  $\Psi_1 + u_1\Psi_2 + 2\nu\frac{\partial\Psi_2}{\partial x_1} = 0$  along  $S_I$  and

$$\begin{aligned} \Psi_1 + 2u_1\Psi_2 + \Phi + 2\nu\frac{\partial\Psi_2}{\partial x_1} &= 0 \\ \frac{\partial\Psi_3}{\partial x_1} + \frac{\partial\Psi_2}{\partial x_2} &= 0 \end{aligned}$$

along  $S_O$ . The above boundary conditions are imposed by modifying the adjoint flux through all the cell faces belonging to  $S_I$  and  $S_O$  as

$$\vec{f}_{S_I}^A = \begin{bmatrix} \Psi_2 \\ u_1 + \Psi_2 \\ \nu(\frac{\partial\Psi_3}{\partial x_1} + \frac{\partial\Psi_2}{\partial x_2}) \end{bmatrix}, \quad \vec{f}_{S_O}^A = \begin{bmatrix} -\Psi_2 \\ \Phi \\ 0 \end{bmatrix}$$

respectively. Finally, the sensitivity derivatives become

$$\frac{\delta F}{\delta b_m} = - \int_0^T \int_{S_w} (\Psi_1 n_i + f_{ik}^{A,vis} n_k) \frac{\partial u_i}{\partial x_l} \frac{\delta x_l}{\delta b_m} dS dt$$

which are computed as in [8].

## 110 5. UQ using Non-Intrusive PCE

Let the QoI  $F(\vec{\xi})$  be, a stochastic function of the stochastic variables  $\vec{\xi}$  associated with the probability density function  $w(\vec{\xi})$  (PDF). A family of orthogonal polynomials  $H_i(\vec{\xi})$ , with  $i$  defining the maximum degree of each polynomial, is defined. In PCE,  $F$  is approximated by a linear combination of  $C + 1 = (N + q)! / (N!q!)$  Hermite polynomials [11, 12, 18],

$$F(\vec{\xi}) \simeq \sum_{i=0}^C a_i H_i(\vec{\xi}) \quad (7)$$

where  $N$  the number of stochastic variables and  $q$  the chaos order. The first two statistical moments of  $F$  (mean value -  $\mu_F$  and variance -  $\sigma_F^2$ ) can be computed as

$$\mu_F = \int_{-\infty}^{+\infty} F(\vec{\xi}) w(\vec{\xi}) d\Omega_{\vec{\xi}}, \quad \sigma_F^2 = \int_{-\infty}^{+\infty} (F(\vec{\xi}) - \mu_F)^2 w(\vec{\xi}) d\Omega_{\vec{\xi}} \quad (8)$$

or, through Galerkin projections,

$$\mu_F = a_0, \quad \sigma_F^2 = \sum_{i=0}^C a_i^2 \quad (9)$$

where  $a_i$  are the PCE coefficients, given by the integrals

$$a_i = \int_{-\infty}^{+\infty} F(\vec{\xi}) H_i(\vec{\xi}) w(\vec{\xi}) d\Omega_{\xi}, \quad i = 0, 1, \dots, C \quad (10)$$

The Gauss quadrature integration formula can be used to compute the above integrals. The  $F$  values at  $M = (q+1)^N$  points  $p_i$  (Gaussian points) are weighted (with known weight  $r_m$ ) and summed up to approximate all integrals in eqs. 10,

$$a_i = \sum_{m=1}^M r_m F(p_m) H_i(\vec{\xi}) \quad (11)$$

The objective function to be maximized for the problems under uncertainties is defined as  $\hat{F} = \mu_F + k\sigma_F^2$ , where  $k$  a user-defined weight ( $k = -1$ , worst case scenario optimization). To perform the optimization with a gradient-based method, the derivatives of the first two statistical moments w.r.t.  $b_m$  are required. Based on eqs. 9 and 10, the following derivatives

$$\frac{\partial a_i}{\partial b_m} = \int_{-\infty}^{+\infty} \frac{\partial F}{\partial b_m}(\vec{\xi}) H_i(\vec{\xi}) w(\vec{\xi}) d\Omega_{\xi}, \quad i = 0, 1, \dots, C \quad (12)$$

are computed, where  $\frac{\partial F}{\partial b_m}$  are computed by the continuous adjoint method. As a consequence,

$$\frac{\partial \mu_F}{\partial b_m} = \frac{\partial a_0}{\partial b_m}, \quad \frac{\partial \sigma_F^2}{\partial b_m} = \sum_{i=0}^C 2a_i \frac{\partial a_i}{\partial b_m} \quad (13)$$

115 These derivatives are, then, used to compute  $\frac{\partial \hat{F}}{\partial b_m}$ . In optimization problems under uncertainties, the first two statistical moments should be computed with  $M$  calls to the CFD software. Furthermore, to compute the derivatives of  $\mu_F$  and  $\sigma_F^2$ , the adjoint problem must be solved for each Gaussian node. Thus, the cost per optimization cycle is  $2M$  equivalent flow solutions (considering that a flow and an adjoint solution have the same cost).

## 6. Applications

120 The aforementioned methods are used to optimize the shape of a diaphragm pump which includes three parts, namely the inlet diffuser, the main body with the diaphragm and the outlet diffuser (fig. 1). Its working principles are similar to the respiratory system of humans. The elastic diaphragm is deformed (by periodically moving up and down) inducing fluid motion to the right, in addition to the effect of the pressure difference between inlet and outlet. When 125 the pump volume is increasing, i.e. the diaphragm moves upwards, more fluid is impelled inside the pump compared to that leaving the pump from the outlet. Conversely, when the diaphragm moves down, the pressure is increased driving fluid to the outlet. The pump characteristics, such as its shape and

130 flow conditions, determine the quantity of backflow at the outlet, which should be kept as low as possible. The diaphragm displacement along  $y$  is given by  $\Delta y = A \sin(2\pi t/T)$ , where the amplitude  $A$  is set to 0.03 times the diaphragm length and the oscillations period ( $T$ ) to 2 *sec*. The inlet and outlet diffuser shapes are controlled by 3 and 4 points, respectively. Their  $x$  and  $y$  coordinates are considered as design variables leading to 14 design variables in total, fig. 1.

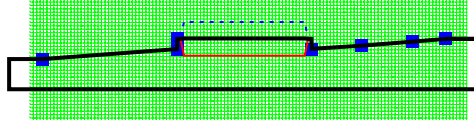


Figure 1: Pump geometry along with the points allowed to be displaced each of them gives two (design variables) marked with squares and the corresponding Cartesian grid. The maximum and minimum positions of the diaphragm are shown with blue and red line, correspondingly.

135 Initially, an optimization without uncertainties is carried out using the cut-cell method and its adjoint to compute the derivatives of the objective function (the QoI, in this case, eq. 4). 33 optimization cycles were performed and the corresponding convergence history is shown in fig. 2a. The objective function  
 140 has increased by  $\sim 0.45\%$ , resulting to an optimal geometry without backflow at the outlet. Due to the fact that the reference geometry produces backflow only at a small part of the outlet, there is not much room for improvement. The differences between the optimal and the reference geometry are shown in fig. 3a and their velocity magnitude iso-areas in figs. 4a and 4b. Fig. 5 gives a blow-up  
 145 view of the part where backflow occurs at the reference geometry.

Regarding the optimizations under uncertainties, two uncertain variables are considered and three different optimization runs were performed. In the first one, the outlet static pressure is the only stochastic variable with mean value  $\mu = 10^5$  Pa and standard deviation  $\sigma = 10$  Pa. The chaos order is  $q =$   
 150 3, requiring evaluations at 4 Gaussian nodes. The convergence history after 14 optimization cycles is presented in fig. 2b. The resulted optimal geometry improves the objective function by  $\sim 0.2\%$ . Fig. 3b shows the reference and optimal geometries. The velocity magnitude iso-areas for the resulted optimal geometry, for the flow at the mean value of the outlet static pressure, is depicted  
 155 in fig. 4c.

In the second optimization problem, the inlet total pressure ( $\mu = 100100$  Pa and  $\sigma = 10$  Pa) is the only stochastic variable and  $q = 3$ . The convergence history after 22 optimization cycles is presented in fig. 2c. The main change in the optimal geometry (fig. 3c) is that the outlet diffuser has been pushed in,  
 160 which result to  $\sim 0.3\%$  improvement. In fig. 4d, the velocity magnitude iso-areas of the optimal geometry, for the flow at the mean value of the inlet total pressure, are plotted.

The third and final optimization problem includes two stochastic variables, both the inlet total pressure ( $\mu = 100100$  Pa,  $\sigma = 10$  Pa) and the outlet static pressure ( $\mu = 10^5$  Pa,  $\sigma = 10$  Pa). 9 Gaussian nodes are necessary for  $q = 2$ . After  
 165 14 optimization cycles, the objective function has increased by  $\sim 0.1\%$  (fig. 2d)

170 which states that more stochastic variables restrict further the optimal solution. The optimal geometry is slightly changed in contrast with the reference one (fig. 3d) and its velocity magnitude iso-areas, for the flow at the mean values of the inlet total and the outlet static pressure, is plotted in fig. 4e. Note that in none of the optimal geometries backflow occurs.

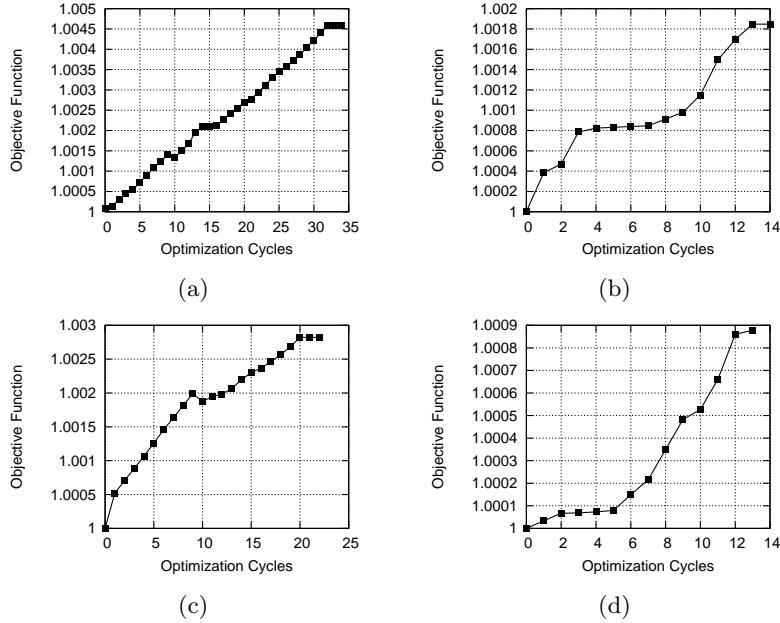


Figure 2: Convergence histories of the optimization (a) without uncertainties, (b) with the outlet static pressure, (c) the inlet total pressure and (d) both of them as uncertain variables.

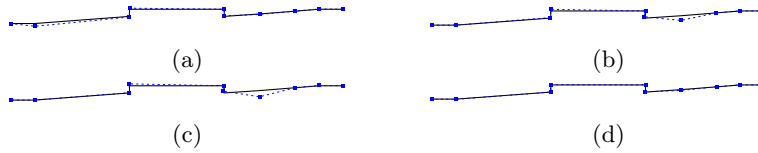


Figure 3: Comparison of the reference (black line) and optimal (blue dashed line) geometries (only the inlet and outlet diffusers are shown) for the optimization cases (a) to (d) as in the caption of fig. 2a.

### Conclusion

175 The cut-cell method for incompressible fluids of unsteady 2D laminar flows in areas with moving boundaries was developed. The discretization of the flow equations is based on the pseudo-compressibility method and the Reynolds theorem for the unsteady term. The developed software was used to solve the flow

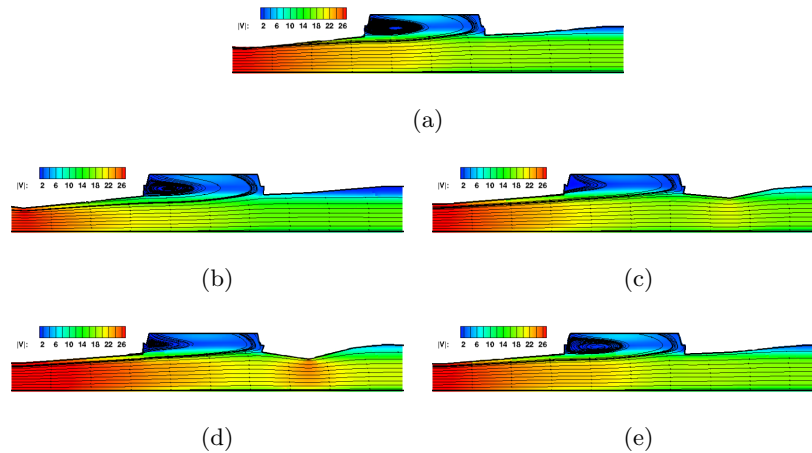


Figure 4: Optimization under uncertainties: Velocity magnitude iso-areas for (a) the reference geometry and geometries optimized (b) without uncertainties, (c) with the outlet static pressure, (d) the inlet total pressure and (e) both of them as stochastic variables. These plots fields correspond computations performed at the mean value of the uncertain flow conditions.

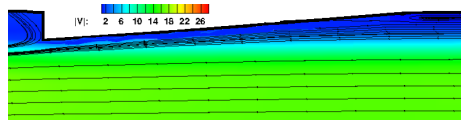


Figure 5: Reference geometry: backflow close to the exit boundary.

inside a diaphragm pump. The corresponding adjoint method was also developed. An optimization was carried out to optimally reshape the inlet and outlet diffusers, eliminating backflow at the exit. The operation of the pump under uncertainties was also studied. The non-intrusive PCE technique was used to compute the mean value and the standard deviation of the QoI. Finally, the PCE technique was differentiated and became part of the optimization process under uncertainties. The resulting algorithm was utilized to optimize the pump shape by choosing three different sets of uncertain variables. In all cases the backflow along the outlet of the optimized geometry was suppressed.

## Acknowledgement

Research presented in this paper has been funded by the Business Plan "Development of Human Resources, Education and Lifelong Learning" entitled "Support Researchers with Emphasis on Young Researchers" with the co-financing of Greece and the European Union. The project title is "Design-Optimization of Diaphragm Pumps under Operational/Manufacturing Uncertainties using the Cut-Cell Method and Polynomial Chaos Expansion". The authors would also like to thank P-I.G.Vrionis for useful contributions.

## References

- 195 [1] E. Stemme, G. Stemme, A valveless diffuser/nozzle-based fluid pump, *Sensors and Actuators A: Physical* 39 (1993) 159 – 167.
- [2] R. Löhner, Adaptive remeshing for transient problems, *Computer Methods in Applied Mechanics and Engineering* 75 (1989) 195 – 214.
- [3] R. Meakin, N. Suhs, Unsteady aerodynamic simulation of multiple bodies  
200 in relative motion (1989).
- [4] R. Mittal, G. Iaccarino, Immersed Boundary Methods, *Annual Review of Fluid Mechanics* 37 (2005) 239–261.
- [5] C. Peskin, Flow patterns around heart valves: a numerical method, *Journal of Computational Physics* 10 (1972) 252–271.
- 205 [6] R. Gaffney Jr., H. Hassan, Euler calculations for wings using Cartesian grids, in: *AIAA Aerospace Sciences Meeting*, American Institute of Aeronautics and Astronautics, Reston, Virginia, 1987.
- [7] D. Clarke, H. Hassan, M. Salas, Euler calculations for multielement airfoils using Cartesian grids, *AIAA Journal* 24 (1986) 353–358.
- 210 [8] K. Samouchos, S. Katsanoulis, K. Giannakoglou, Unsteady adjoint to the cut-cell method using mesh adaptation on GPUs, in: *ECCOMAS Congress*, Crete Island, Greece, 2016.
- [9] S. Asmussen, P. Glynn, *Stochastic simulation: Algorithms and analysis*, in: *Stochastic Modelling and Applied Probability*. Springer New York, 2007.
- 215 [10] E. Papoutsis-Kiachagias, D. Papadimitriou, K. Giannakoglou, Robust design in aerodynamics using 3rd-order sensitivity analysis based on discrete adjoint. Application to quasi-1d flows, *International Journal for Numerical Methods in Fluids* 69 (2012) 691–709.
- [11] S. Poles, V. Desai, A polynomial chaos approach to robust multiobjective optimization, *Hybrid and Robust Approaches to Multiobjective Optimization*, Dagstuhl Seminar Proceedings (2009).  
220
- [12] M. Eldred, J. Burkardt, Comparison of non-intrusive Polynomial Chaos and stochastic collocation methods for uncertainty quantification, in: *American Institute of Aeronautics and Astronautics*, 2009.
- 225 [13] E. Papoutsis-Kiachagias, K. Giannakoglou, Continuous adjoint methods for turbulent flows, applied to shape and topology optimization: industrial applications, *Archives of Computational Methods in Engineering* 23 (2016) 255–299.

- 230 [14] H. Ji, F.-S. Lien, E. Yee, A new adaptive mesh refinement data structure with an application to detonation, *Journal of Computational Physics* 229 (2010) 8981 – 8993.
- [15] A. Chorin, A numerical method for solving incompressible viscous flow problems, *Journal of Computational Physics* 2 (1967) 12 – 26.
- 235 [16] E. Turkel, Preconditioned methods for solving the incompressible and low speed compressible equations, *Journal of Computational Physics* 72 (1987) 277 – 298.
- [17] P. Roe, Approximate Riemann solvers, parameter vectors, and difference schemes, *Journal of Computational Physics* 43 (1981) 357–372.
- 240 [18] D. Xiu, G. Karniadakis, The Wiener-Askey polynomial chaos for stochastic differential equations, *Arch. Comput. Methods Eng.* 24 (2002) 619–644.